

Impact of Numerical Settings on Simulation Performance of the Gamma-Re-Theta Model for 2D and 3D Bluff Body Transitional Flow Cases using OpenFOAM

Sumedh Soman¹, Ashley Melvin², Divyesh Variya², and Janani Srree Murallidharan³

¹Department of Mechanical Engineering, KJ Somaiya College of Engineering, Mumbai-400077, India

²FOSSEE, IIT Bombay, Mumbai-400076, India

³Department of Mechanical Engineering, IIT Bombay, Mumbai-400076, India

ABSTRACT

Modeling transitional turbulence, especially over bluff bodies, has always been difficult due to the various mechanisms governing transition depending upon the nature of the flow. However, these flows are equally vital in several aerodynamic analyses, and therefore it is imperative to simulate these flows accurately. The Gamma-Re-Theta model (Local Correlation- based Transition Model) is a turbulence model designed to simulate transitional turbulence and is based upon the k-Omega SST model. However, the simulation performance of this model depends upon numerical settings, and the correct setup is vital to achieving accurate results. Here we analyze the impact of multiple numerical simulation parameters on the performance of the Gamma-Re-Theta model for a 2D as well as a 3D case and find the configuration which produces the best results. It was found that the linear upwind divergence scheme coupled to the Geometric Algebraic Multigrid (GAMG) solvers produced the best results in both cases.

Keywords: Transitional Turbulence, Simulation, Numerical Schemes, bluff body flows, OpenFOAM

1. INTRODUCTION

Transitional turbulence has traditionally been difficult to simulate as the mechanism of transition differs depending upon the nature of the flow [1]. Analysis of bluff body flows is an important part of aerodynamics and several applications involve simulating transitional flows. The Gamma-Re-Theta transitional turbulence model, formally known as the Local Correlation Based Transition model (LCTM), devised by Langtry, Menter *et al.* [2] is a RANS-based transitional turbulence model. This model was built upon the k-Omega SST model and involves solving two additional equations for two nonphysical quantities designed to predict the onset of turbulence. This model has the advantage of being able to accommodate multiple transition mechanisms as well as being able to handle re-laminarization. Furthermore, since the model does not involve nonlocal calculations, it can be run on modern CFD solvers relying on domain decomposition to run on several processor cores at once. However, the performance of the transitional turbulence model is also heavily dependent upon the numerical scheme being utilized. Finding the correct

set of numerical schemes to use, therefore, becomes imperative. This study focuses on two bluff body flow cases, the ERCOFTAC T3A case (flow over a flat plate), and flow over a spherical body.

2. LITERATURE REVIEW AND OBJECTIVE

The objective of this study is to analyze the impact of numerical settings on the overall simulation performance. Rizzo *et al.* [5] coupled the Gamma-Re-Theta model to the Spalart-Allmaras model and validated it on bluff body flows. It was found that the given combination was beneficial in reducing the computational cost without adversely affecting simulation performance. The T3A ERCOFTAC case was chosen as the first simulation case. Wall shear stress plots with respect to local Reynolds number were obtained via experiment, by Coupland [6]. Savill [13] simulated the flow using a variety of closure models. The second case chosen was flow over a sphere, which is a 3D flow case. Nakhostin *et al.* [4] simulated flow over sphere using the Gamma-Re-Theta model on OpenFOAM and compared the results with wind tunnel experiment values. It was found that the results matched better with experimental values as compared to the k-Omega SST model, which simulates fully turbulent flow, but there was still considerable deviation. Also, the simulation diverged for higher Reynolds numbers. Robertson *et al.* [3] performed an extensive study for 2D as well as 3D bluff body flows using a variety of turbulence models, divergence schemes, and pressure-velocity coupling algorithms on OpenFOAM. RANS and hybrid RANS-LES models were tested for a backward-facing step, a sphere, and also a delta wing at various angles of attack. It was found that the 2nd order linear upwind divergence scheme was the best simulation scheme available for RANS turbulence models, and the SIMPLE algorithm was determined to be the optimal pressure velocity coupling algorithm. Amongst RANS models, the k-Omega SST model was deemed to be the best turbulence model. The findings of this study were used as the baseline for the present study.

In the given study, the T3A ERCOFTAC case, as well as the flow over a sphere case, are simulated on OpenFOAM, and multiple simulation schemes were tested, to determine the optimum configuration for modeling bluff body transitional

flows, and analyze the impact of each numerical scheme on the overall simulation performance.

3. MATERIALS AND METHODS

The numerical parameters to be tested were broadly classified into three categories, divergence schemes, pressure-velocity coupling algorithms, and linear equation solvers. Divergence schemes numerically approximate the divergence of a flux, which is essentially the net rate of change of a flux as a function of space. Pressure-Velocity coupling algorithms are used to predict the velocity field and consequently compute the convection of pressure, which is a scalar variable.

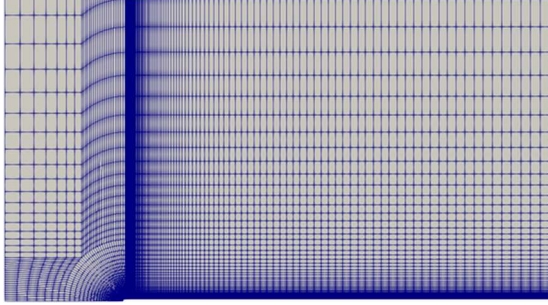


Figure 1: Diagram of the mesh for the flat plate case.

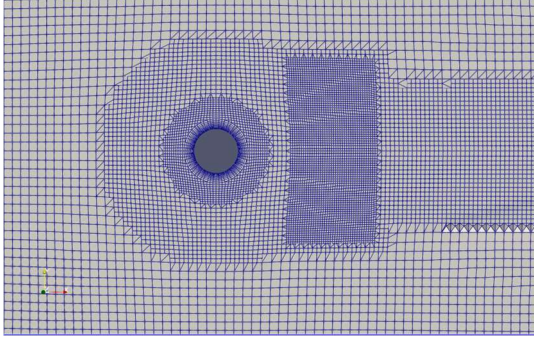


Figure 2: Diagram of the mesh for the sphere case.

3.1 Geometry and Mesh

The geometry for the flat plate case was implemented as per the ERCOFTAC T3A case dimensions [6], involving a 1700 mm long plate with 20 mm height, and a leading edge with a 15 mm diameter. A tutorial for the T3A case is available in OpenFOAM documentation, and the geometry and mesh were carried over from the same [15]. Figure 1 depicts the mesh generated over the domain. For the sphere case, the geometry and mesh used by Nakhostin [4] were followed. A 20mm diameter sphere geometry was created and a domain of size $20D \times 10D \times 10D$, where D is the diameter of the sphere, was created. The mesh for the sphere was created using the snappyHexMesh utility available in OpenFOAM, but with modifications to the mesh created by Nakhostin. Figure 2 displays the mesh generated over the geometry. Additional refinement was applied near the surface of the sphere, and on the refinement regions, and 15 surface layers were used in the refinement region. This altered the y^+

values but helped reduce computational time without affecting the simulation results adversely.

3.2 Governing Equations

The governing equations of the gamma-re-theta model are as follows [2]

$$\begin{aligned} \frac{\partial(\rho\gamma)}{\partial t} + \frac{\partial(\rho u_j \gamma)}{\partial x_j} &= P_\gamma - E_\gamma \\ &+ \frac{\partial}{\partial x_j} \left[\left(\mu + \frac{\mu_t}{\sigma_f} \right) \frac{\partial \gamma}{\partial x_j} \right] \end{aligned} \quad (1)$$

$$P_\gamma = F_{length} c_{a1} \rho S [\gamma F_{onset}]^{0.5} (1 - \gamma) \quad (2)$$

$$\begin{aligned} \frac{\partial(\rho \overline{Re_{\theta t}})}{\partial t} + \frac{\partial(\rho u_j \overline{Re_{\theta t}})}{\partial x_j} &= P_{\theta t} \\ &+ \frac{\partial}{\partial x_j} \left[\sigma_{\theta t} (\mu + \mu_t) \frac{\partial \overline{Re_{\theta t}}}{\partial x_j} \right] \end{aligned} \quad (3)$$

$$P_{\theta t} = c_{\theta t} \frac{\rho}{t} (Re_{\theta t} - \overline{Re_{\theta t}}) (1.0 - F_{\theta t}) \quad (4)$$

$$t = \frac{500\mu}{\rho U^2} \quad (5)$$

$$\begin{aligned} \frac{\partial(\rho k)}{\partial t} + \frac{\partial(\rho u_j k)}{\partial x_j} &= \tilde{P}_k - \tilde{D}_k \\ &+ \frac{\partial}{\partial x_j} \left[(\mu + \sigma_k \mu_t) \frac{\partial k}{\partial x_j} \right] \end{aligned} \quad (6)$$

$$\begin{aligned} \frac{\partial(\rho \omega)}{\partial t} + \frac{\partial(\rho u_j \omega)}{\partial x_j} &= \frac{\alpha}{\vartheta_t} P_k - D_\omega + C d_\omega \\ &+ \frac{\partial}{\partial x_j} \left[(\mu + \sigma_\omega \mu_t) \frac{\partial \omega}{\partial x_j} \right] \end{aligned} \quad (7)$$

$$\tilde{P}_k = \gamma_{eff} P_k \quad (8)$$

$$\mu_t = \left[\frac{\rho k}{\omega}; \frac{a_1 \rho k}{S F_2} \right] \quad (9)$$

(1) is a transport equation for γ (intermittency), which is a non-physical quantity whose value varies between zero and one, and it triggers or halts the production of turbulent kinetic energy, as can be seen in (8), and (2) describes the source

terms of the intermittency transport equation, which triggers intermittency production based on empirical correlations. (3) is a transport equation for transition momentum thickness Reynolds number. At this Reynolds number, the boundary layer profile begins transitioning towards a turbulent profile. It is downstream of the critical momentum thickness Reynolds number, which is when the boundary layer assumes a turbulent profile. The transition momentum thickness Reynolds number can be computed in the free stream using an empirical correlation involving turbulent intensity, but cannot be computed in the boundary layer, which is why a transport equation was needed. The source terms of (3), described in (4) and (5) are designed in such a way that the freestream values of the transition momentum thickness Reynolds number diffuse into the boundary layer. (6) and (7) are transport equations for the turbulent kinetic energy and specific dissipation rate, and (8) and (9) detail the source terms of both equations respectively. (7) and (9) are based upon an improved version of the k-Omega SST model, as described in [14].

3.3 Divergence Schemes

Three divergence schemes were tested for both cases. Linear Upwind can be expressed for unsteady-state convection as [7]

$$\begin{aligned} \phi_j^{i+1} &= 0.5(\phi_j^{i+1} + \phi_j^i) \\ &- 0.5 \frac{\Delta t}{\Delta x} [\epsilon_j F_j^n \\ &- (\epsilon_j - \epsilon_{j-1}) F_{j-1}^n + \epsilon_{j-1} F_{j-2}^n] \\ &- 0.5 \frac{\Delta t}{\Delta x} [-\epsilon_{j-1} F_{j-1}^{n+1} \\ &- (\epsilon_j - \epsilon_{j-1} - 1) F_j^{n+1} \\ &+ (1 - \epsilon_{j-1}) F_{j+1}^{n+1}] \end{aligned} \quad (10)$$

where ϕ is any field of interest. Also,

$$(\epsilon_j, \epsilon_{j-1}) = \begin{cases} (0,0) & \text{MacCormack scheme} \\ (0,1) & \text{MU transition operator} \\ (1,0) & \text{UM transition operator} \\ (1,1) & \text{Upwind scheme} \end{cases} \quad (11)$$

The upwind scheme, for a given flux ϕ can be expressed as [8]

$$a_j \phi_j = a_{j-1} \phi_{j-1} + a_{j+1} \phi_{j+1} \quad (12)$$

where,

$$a_{j-1} = \left(\frac{\Gamma}{dx} \right)_{j-\frac{1}{2}} + \max\left(\rho u_{j-\frac{1}{2}}, 0\right) \quad (13)$$

$$a_{j+1} = \left(\frac{\Gamma}{dx} \right)_{j+\frac{1}{2}} - \max\left(-\rho u_{j+\frac{1}{2}}, 0\right) \quad (14)$$

Here, Γ denotes the diffusivity coefficient.

The QUICK scheme can be expressed as [9]

$$a_j \phi_j = a_{j-1} \phi_{j-1} + a_{j+1} \phi_{j+1} + a_{j-2} \phi_{j-2} + a_{j+2} \phi_{j+2} \quad (15)$$

where,

$$a_j = a_{j-1} + a_{j+1} + a_{j+2} + a_{j-2} + \left(\rho u_{j+\frac{1}{2}} - \rho u_{j-\frac{1}{2}} \right) \quad (16)$$

$$\begin{aligned} a_{j-1} &= \left(\frac{\Gamma}{dx} \right)_{j-\frac{1}{2}} + 0.75 \alpha_{j-\frac{1}{2}} \left(\rho u_{j-\frac{1}{2}} \right) \\ &+ 0.125 \alpha_{j+\frac{1}{2}} \left(\rho u_{j+\frac{1}{2}} \right) \\ &- 0.375 (1 - \alpha_{j-\frac{1}{2}}) \rho u_{j-\frac{1}{2}} \end{aligned} \quad (17)$$

$$a_{j-2} = -0.125 \alpha_{j-2} \rho u_{j-2} \quad (18)$$

$$\begin{aligned} a_{j+1} &= \left(\frac{\Gamma}{dx} \right)_{j+\frac{1}{2}} - 0.375 \alpha_{j+\frac{1}{2}} \left(\rho u_{j+\frac{1}{2}} \right) \\ &- 0.75 \alpha_{j+\frac{1}{2}} \left(\rho u_{j+\frac{1}{2}} \right) \\ &- 0.125 (1 - \alpha_{j-\frac{1}{2}}) \rho u_{j+\frac{1}{2}} \end{aligned} \quad (19)$$

$$a_{j+2} = 0.125 (1 - \alpha_{j+\frac{1}{2}}) \rho u_{j+\frac{1}{2}} \quad (20)$$

$$\begin{aligned} \alpha_{j-\frac{1}{2}} &> 0 \text{ for } \rho u_{j-\frac{1}{2}} > 0, \alpha_{j+\frac{1}{2}} < 0 \text{ for } \rho u_{j+\frac{1}{2}} < 0 \\ \alpha_{j+\frac{1}{2}} &> 0 \text{ for } \rho u_{j+\frac{1}{2}} > 0, \alpha_{j-\frac{1}{2}} < 0 \text{ for } \rho u_{j-\frac{1}{2}} < 0 \end{aligned} \quad (21)$$

3.4 Pressure Velocity Coupling algorithms

Two pressure velocity coupling algorithms were tested. The simpleFoam solver, which is based on the SIMPLE algorithm proposed by Patankar *et al.* [10] was the first algorithm tested. The other algorithm being pimpleFoam, which is based upon the PIMPLE algorithm which in itself is a blend of PISO and SIMPLE. Essentially the SIMPLE algorithm is run for each time step.

3.5 Linear Equation Solvers

Two combinations of solvers were tested. The first combination involved using Gauss-Seidel solvers for all fields except pressure, which was solved using multigrid solvers. The second combination employed Multigrid solvers (GAMG) for all variables.

3.6 Boundary Conditions

All the walls in the simulation were assigned slip boundary conditions, in order to ensure that only momentum and energy transfer can take place. The turbulent kinetic energy at inlet was estimated as

$$k_{inlet} = \frac{3}{2} (UI)^2 \quad (22)$$

where U is the velocity and I is the turbulence intensity at the inlet. The specific dissipation rate at the inlet was calculated using the following equation

$$\omega = \frac{C_\mu^{\frac{3}{4}} k^{\frac{1}{2}}}{l} \quad (23)$$

C_μ is a constant whose value is equal to 0.09, k is the turbulent kinetic energy, and l is the turbulent length scale.

4. RESULTS AND DISCUSSION

Both the cases were run with multiple configurations as mentioned in the previous sections, and the results were plotted. For the T3A case, wall shear stress was deemed to be the variable of interest, and for the sphere case, the coefficient of drag (C_d) was chosen as the variable to be analyzed, along with velocity contours. The results are explained in the below subsections.

4.1 Wall Shear Stress over plate length

Figure 3 depicts the variation of wall shear stress with respect to the plate length, for the T3A plate case. It can be seen from the data that the linear upwind scheme is the best performing scheme here, predicting the wall shear stress with remarkable accuracy throughout the length of the plate. Linear Upwind scheme is very effective at eliminating spurious oscillations occurring at discontinuities, due to its ability to switch between MacCormack scheme and second order Upwind. Furthermore, both the constituent schemes are second order in nature, further enhancing accuracy. The Upwind divergence scheme also predicts accurate wall shear stress magnitude values except at the leading edge of the plate, where the predicted value is considerably higher than experimental values. This can be attributed to the upwind scheme being first order, and also not having any special provisions to deal with discontinuities. Although the leading-edge wall shear stress values for QUICK are better than those predicted by Upwind, overall, the values deviate noticeably from experimental values. QUICK is prone to overshoots and undershoots [11], which may be the cause of the inaccurate results. The simulation with QUICK divergence scheme also did not converge, even within 1000 iterations, and the residuals kept fluctuating. QUICK has negative coefficients in its formulation, and stability issues have been observed due to the same. These observed stability issues might be the reason for the simulation not converging.

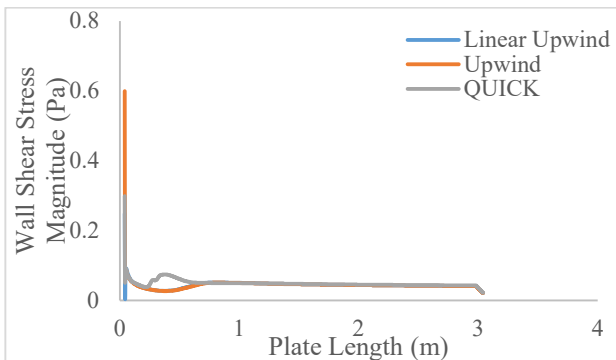


Figure 3: Variation of Wall shear stress with respect to plate length for different divergence schemes.

Figure 4 displays the variation of the wall shear stress magnitude with respect to the plate length, for different solver setups. pimpleFoam works on the PIMPLE algorithm, which is a blend of SIMPLE and PISO algorithms. It is a transient solver, as opposed to simpleFoam. Essentially, the SIMPLE algorithm is run for each time step multiple times. The nOuterCorrectors parameter specifies the number of times the SIMPLE algorithm is to be run for each time step. This algorithm, being transient, is much more likely to diverge, and consequently one needs to pay attention to residual control and relaxation coefficients. The model converged after extensive tuning, but the time required for computation was much higher as compared to the simpleFoam case, with both configurations giving the same output.

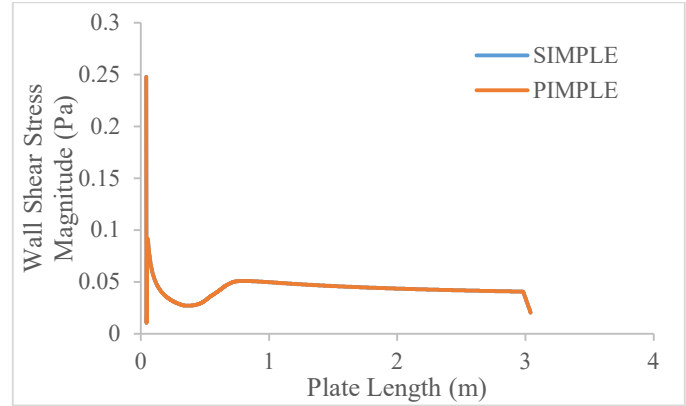


Figure 4: Variation of Wall shear stress with respect to plate length for different pressure velocity coupling algorithms.

Figure 5 shows the variance of the wall shear stress with respect to plate length for two different solver configurations. It is visible that the plots are identical. However, the simulation setup using Multigrid solvers to solve for all equations converged in 193 iterations, while the setup using Multigrid solvers to solve only for pressure converged in 269 iterations. This can be attributed to the ability of Multigrid equation solvers to annihilate short as well as long-wavelength errors, ensuring a faster rate of convergence.

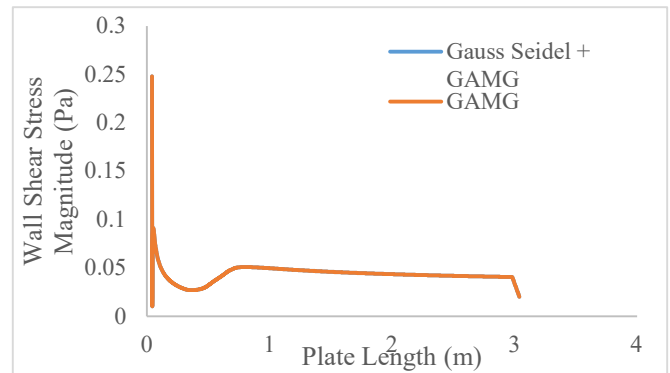


Figure 5: Variation of Wall shear stress with respect to plate length for different solvers.

4.2 Coefficient of Drag for sphere

Figure 6 shows the variance of C_d over different Reynolds numbers for linear upwind and upwind divergence schemes. These C_d values were recorded once the C_d value had converged to 3 significant digits. On comparing with experimental results of Achenbach [12] it is seen that the C_d values overall follow a similar trend. For Reynolds numbers 2×10^5 and 2.5×10^5 , the simulation is deviating from the trend. With additional refinements, we think that simulation values for these Reynolds numbers can be improved. For all Reynolds number values in the simulation, the C_d never converges due to vortex shedding, especially since the flow is transitional. When the upwind divergence scheme was used in the simulations, the C_d did not converge at all, and for higher Reynolds number values, the simulation began to diverge. Also, the wake region predicted by upwind is grossly inaccurate, because it is predicting a very small wake region, which implies that the boundary layer does not separate from the surface of the sphere. The wake region predicted by upwind can be seen in Figure 7.

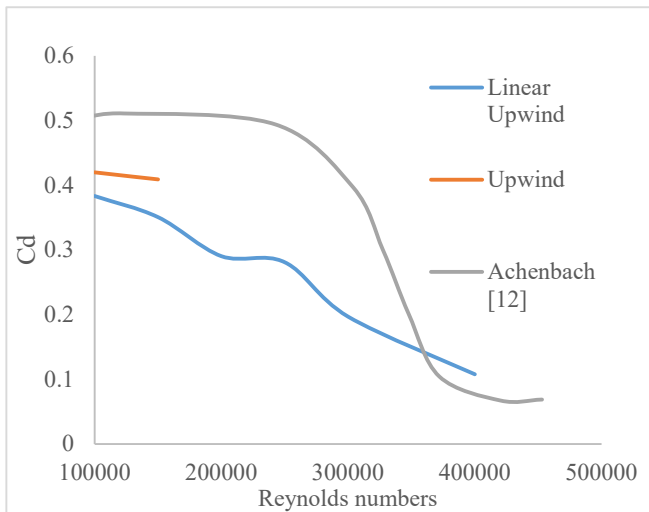


Figure 6: Variation of C_d of sphere with Reynolds number.

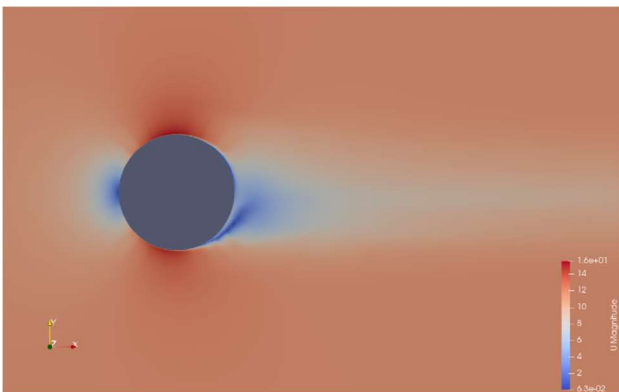


Figure 6: Wake region for simulation employing upwind divergence scheme.

4.3 Comparison with pimpleFoam

The given case setup was also run using the pimpleFoam algorithm, which is a transient solver. Since the given scheme is transient, the Courant number at each timestep must not exceed 1, and therefore, appropriately small time-steps had to be selected. The simulation had reached 0.2 s on running for 48 hours, on a system with 10 CPU cores. The C_d values had not converged till that time step. Figure 7 shows the variation of C_d with respect to the time step for pimpleFoam. As can be seen from the data, no trends can be deduced. But since transitional flow is transient in nature, one is led to assume that pimpleFoam might be better suited for the given simulation. The given simulation needs more run time to make an informed decision regarding usage of this pressure-velocity coupling algorithm.

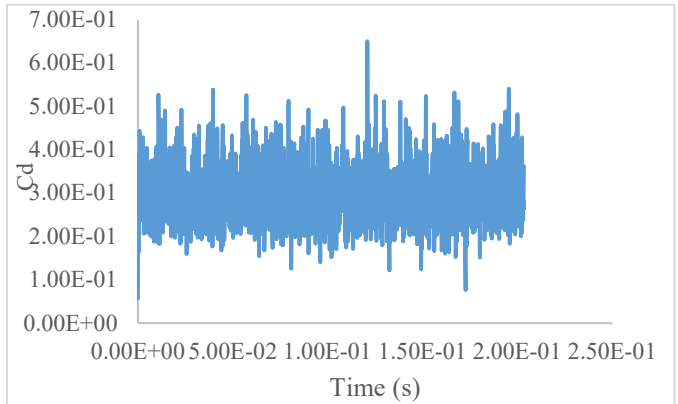


Figure 6: Wake region for simulation employing upwind divergence scheme.

5. CONCLUSIONS

In this study, we have analyzed the performance of the Gamma-Re-Theta model with respect to various numerical schemes using OpenFOAM. Here we find that the Linear Upwind scheme proves to be the best divergence scheme for both bluff body flows, due to the second-order nature of both the divergence schemes and also the ability of the divergence scheme to switch between MacCormack and Upwind divergence schemes, eliminating spurious oscillations at discontinuities and transition regions, verifying results shown by Robertson *et al.* [3]. Amongst linear equation solvers, GAMG proves to be the most effective linear equation solver, due to its ability to annihilate both short and long wavelength errors. It is recommended to use GAMG for all variables for a quicker rate of convergence and also for stability. pimpleFoam is not justified for the plate flow case, as the computational cost is too high. Amongst Pressure-Velocity coupling algorithms, simpleFoam (SIMPLE) is the best choice for the T3A case, as pimpleFoam does not improve upon the results but rather increases computational cost. For the sphere case, a firm conclusion cannot be delivered due to the solution not being allowed to run for a sufficient time period. More runtime will be needed to decide whether pimpleFoam can be considered for this case.

ACKNOWLEDGEMENTS

The authors would like to thank the FOSSEE project, IIT Bombay for its financial support of this research. First author would like to thank the second authors for their constant support, guidance and encouragement throughout. The authors would also like to thank Ms. Swetha for her valuable inputs during discussions.

NOMENCLATURE

γ	Intermittency	--
Re_{θ_t}	Transition Momentum thickness	--
	Reynolds number	
C_D	Drag coefficient	--
k	Turbulent kinetic energy	[J/kg]
ρ	Density	[kg/m ³]
ω	Specific Dissipation rate	[1/s]
ν_t	Eddy Viscosity	[m ² /s]
μ	Dynamic Viscosity	[Pa-s]

REFERENCES

- [1] Kundu, Pijush K., Ira M. Cohen, and D. Dowling. "Fluid Mechanics 4th." (2008): 1-277.
- [2] Menter, F. R., R. Langtry, and S. Völker. "Transition modelling for general purpose CFD codes." *Flow, turbulence and combustion* 77, no. 1-4 (2006): 277-303.
- [3] Robertson, E., V. Choudhury, S. Bhushan, and D. Keith Walters. "Validation of OpenFOAM numerical methods and turbulence models for incompressible bluff body flows." *Computers & Fluids* 123 (2015): 122-145.
- [4] Nakhostin, S. M., and K. E. T. Giljarhus. "Investigation of transitional turbulence models for CFD simulation of the drag crisis for flow over a sphere." In *IOP Conference Series: Materials Science and Engineering*, vol. 700, no. 1, p. 012007. IOP Publishing, 2019.
- [5] Rizzo, Fabio, V. D'Alessandro, S. Montelpare, and L. Giammichele. "Computational study of a bluff body aerodynamics: Impact of the laminar-to-turbulent transition modelling." *International Journal of Mechanical Sciences* 178 (2020): 105620.
- [6] Coupland J.: ERCOFTAC special interest group on laminar to turbulent transition and retransition: T3a and t3b test cases, Tech. rep., ERCOFTAC, 1990
- [7] Warming, R. F., and Richard M. Beam. "Upwind second-order difference schemes and applications in aerodynamic flows." *AIAA Journal* 14, no. 9 (1976): 1241-1249.
- [8] Spalding, Dudley Brian. "A novel finite difference formulation for differential expressions involving both first and second derivatives." *International Journal for Numerical Methods in Engineering* 4, no. 4 (1972): 551-559.
- [9] Leonard, B. P. "The QUICK algorithm-A uniformly third-order finite-difference method for highly convective flows." *Computer methods in fluids* (1980): 159-195.
- [10] Patankar, Suhas V. *Numerical heat transfer and fluid flow*. CRC press, 2018.
- [11] Versteeg, H. K., and W. Malalasekera. "Computational fluid dynamics." *The finite volume method* (1995)
- [12] Achenbach, Elmar. "Experiments on the flow past spheres at very high Reynolds numbers." *Journal of fluid mechanics* 54, no. 3 (1972): 565-575.
- [13] Savill, A.M. "Some recent progress in the turbulence modelling of by-pass transition", *Near-Wall turbulent flows*, (1993), 829-848
- [14] Menter, F.R.: "Two-equation Eddy-viscosity turbulence models for engineering applications". *AIAA J.* 32(8), 1598–1605 (1994)
- [15] OpenFOAM User Guide- "Turbulence Transition T3A", accessed July 10, 2021
<https://www.openfoam.com/documentation/guides/latest/doc/verification-validation-turbulent-t3a.html>